Journal of Nuclear Materials 392 (2009) 264–271

Contents lists available at ScienceDirect

Journal of Nuclear Materials

journal homepage: www.elsevier.com/locate/jnucmat

IGSCC of grain boundary engineered 316L and 690 in supercritical water

E.A. West *, G.S. Was

University of Michigan, 2355 Bonisteel Boulevard, Ann Arbor, MI 48109, USA

A B S T R A C T

This study evaluated the influence of a high fraction of special grain boundaries on the intergranular stress corrosion cracking susceptibility of 316L stainless steel and nickel base alloy 690 in supercritical water. By thermomechanically processing the alloys to create specimens with largely different special boundary fractions, it was possible to isolate the effects of the grain boundary structure on the intergranular stress corrosion cracking behavior. Constant extension rate tensile experiments were performed in 500 °C deaerated supercritical water, and SEM analysis of the cracking behavior was performed on the gage surfaces of the specimens. Results indicate that the fraction of cracked grain boundary length in the specimens with higher fractions of special boundaries is reduced for 316L and 690 by factors of 9 and 5 at 15% strain, and 3 and 2 at 25% strain, respectively. This reduction is due to the special boundaries, which at 25% strain have a frequency of cracking that is 9–18 times lower than that for a random high angle boundary.

1. Introduction

A growing body of literature shows that many of the candidate alloys for the supercritical water reactor (SCWR) concept are susceptible to intergranular stress corrosion cracking (IGSCC) [1]. This problem is especially evident in the austenitic stainless steels and nickel-base alloys. Teysseyre et al. [2] showed that 316L stainless steel and nickel-base alloy 690 were susceptible to IGSCC in deaerated SCW at temperatures of 400 and 500 °C, and the extent of the cracking increased with irradiation damage. The lower weight gain of the austenitic stainless steels and nickel-base alloys compared to the ferritic–martensitic steels makes them favorable for use as internal core components in the SCWR. The austenitic stainless steels generally form an oxide structure containing an outer layer of magnetite and chromium rich inner layer that is either an iron–chromium spinel or a hematite structured iron chromium oxide, and an internal oxidation layer is also present between the inner oxide layer and base metal [1]. The difference in oxidation behaviors of austenitic and ferritic–martensitic steels is illustrated by comparing the weight gain of D9 and HCM12A exposed to 600 °C SCW for 1026 h [1], where it was shown that the oxidation was roughly a factor of four larger for the ferritic–martensitic steel, HCM12A. Under these same conditions, the weight gain of nickel-base alloy 625 was a factor of three lower than austenitic stainless steel 316 [1]. The successful utilization of the austenitic alloys in the SCWR, however, hinges on the ability to improve their cracking behavior.

IGSCC is heterogeneous in nature, as the susceptibility of a grain boundary depends on local chemical conditions, stress state, and structure. The coincident site lattice (CSL) model [3] is commonly used to characterize the structures of grain boundaries. The boundary is assigned a number corresponding to the reciprocal density of the coinciding lattice sites. The allowed deviations from exact coincidence are defined by Brandon's criterion [4]. The CSLBs as well as low angle boundaries (LABs) which have misorientations of <15° are often referred to as 'special' due to their observed resistance to precipitation and segregation [5–9], intergranular corrosion [10–13], and intergranular cracking [8,14–18] compared to random high angle boundaries (RHAB)s.

The concept of grain boundary engineering (GBE) was first proposed by Watanabe in the early 1980s [19]. Since then, this concept has developed into a method used to reduce all types of grain boundary degradation through the development of alloy treatments that produce high special boundary fractions. These high special boundary fractions are achieved through strain-annealing or strain-recrystallization treatments. In addition to the fraction of special boundaries, the connectivity of the RHAB network is believed to be a key factor in preventing intergranular degradation [20–22]. The propagation of a crack, for example, would be hindered if the connectivity of the RHABs was disturbed by the substitution of special boundary segments.

The IGSCC problems encountered with austenitic alloys in the nuclear industry motivated researchers to study the effectiveness of GBE in improving cracking behavior in high temperature aqueous environments. Researchers demonstrated (1) that special boundaries are resistant to IGSCC and (2) IGSCC can be reduced through GBE. Palumbo et al. [16] performed an experiment on C-rings of alloy 600 in a 10% NaOH environment at 350 °C. It was

* Corresponding author. Tel.: +1 734 936 0266; fax: +1 734 763 4540.
E-mail address: eawest@umich.edu (E.A. West).

0022-3115/$ - see front matter © 2009 Elsevier B.V. All rights reserved.
doi:10.1016/j.jnucmat.2009.03.008

discovered that 58% of the RHABs cracked, while only 12% of the special boundaries (meeting Brandon's criterion) cracked. Pan et al. [15] performed experiments on alloy X-750 compact tension specimens in deaerated 360 °C water. Although there were 818 triple junctions along the path of the crack, none of the encountered LABs or Σ3 boundaries cracked. Crawford and Was [17] showed that the IG cracking behavior of pure Ni–16Cr–9Fe could be improved through GBE in both a 360 °C argon environment and in deaerated, high-purity water. They found that the fraction of boundaries cracked in the GBE specimens ranged from 1 to 8%, while 7–10% of the boundaries in the annealed specimens cracked. They suggested that the resistance of the special boundaries may be due to their ability to transmit lattice dislocations rather than absorb them. Alexandreanu et al. [8] successfully reduced IGSCC in Ni–16Cr–9Fe–xC alloys via GBE in a simulated primary water environment at 360 °C. They found that irrespective of the alloy, microstructure, and strain, the total cracked fraction of boundaries decreased as the CSLB fraction increased. These studies demonstrate that a high fraction of crack resistant boundaries can improve the IGSCC behavior of alloys in high temperature aqueous environments.

Research on the performance of GBE alloys in SCW is limited. Tan et al. [23,24] applied GBE treatments to alloys 800H and 617 prior to exposure in 500 and 600 °C SCW. Compared to their annealed conditions, the GBE specimens had more compact and continuous oxide scales. This was attributed to the lower diffusivity of the low-Σ boundaries compared to the RHABs which made the grain boundary diffusivity as a whole closer to the bulk diffusivity. The only study to date on IGSCC of GBE alloys in SCW was done by Gupta et al. [25] on ferritic–martensitic alloy HT-9. In this study the observed mitigation of IGSCC was attributed to a reduction in precipitate coarsening at the CSLBs and LABs due to the lower diffusivities along these boundaries.

This paper evaluates the influence of a high special boundary fraction on the IGSCC susceptibility of 316L and 690 in SCW. Thermomechanical processing treatments were used to create a nominal, and a grain boundary engineered condition of each alloy. By comparing the cracking behaviors of each condition and determining the character of the boundaries that cracked, the ability to improve the IGSCC behavior of 316L and 690 was determined.

2. Experiment

2.1. Sample preparation

SCWR candidate alloys, 316L stainless steel and alloy 690, were selected for this study based on their previously demonstrated susceptibility to IGSCC in SCW [2]. Their chemical compositions are given in Table 1. The cracking behavior of each alloy was evaluated in two conditions, distinguished by the application of grain boundary engineering; 316L, 316LGBE, 690, and 690GBE. The as-received plate of 316L was annealed at 1100 °C for 20 min followed by a water quench. Both types of specimens were machined from this plate, and the 316L specimen was used in this condition. The 316LGBE specimen was compressed by 5% followed by a 72 h anneal at 967 °C and water quenched, a treatment very similar to that used by Michiuchi et al. [13]. The as-received plate of 690 had been hot rolled at 982–1149 °C, annealed for 25 min at 1038–1093 °C, and air cooled. The 690GBE specimens were machined from this plate and then annealed at 1050 °C for 5 min and water quenched. A portion of the as-received plate was cold-rolled 66%, annealed at 1100 °C for 2 h, and water quenched. The 690 specimens were machined from the plate in this condition. The resulting average grain sizes of the 316L, 316LGBE, 690, and 690GBE specimens in the rolling directions were 51, 170, 29, and 21 μm, respectively.

The tensile specimens were fabricated via electric discharge machining. The specimens were mechanically polished with SiC abrasive paper to 4000 grit and then electropolished in a 10% perchloric acid –90% methanol solution to remove the thin damage layer induced by mechanical polishing. The 316L and 690 specimens were electropolished at 30 V for 15–20 s at temperatures of −50 and −30 °C, respectively, to achieve a mirror finish. Prior to straining, the samples were lightly electro-etched in a 10% oxalic acid in methanol solution for 15 s at 4 V to verify that no grain boundary chromium carbides were present. This etching treatment was demonstrated to reveal grain boundary chromium carbides when present, but was light enough that it did not disturb the mirror finish of the specimens. SEM analysis following etching showed no visible signs of surface degradation.

2.2. Grain boundary character mapping

A Philips XL30FEG SEM equipped with a TexSEM Laboratories orientation imaging microscopy (OIM) system was used to generate grain boundary character maps of the gage surfaces of the specimens. The maps covered over 1000 grains on each specimen, with the exception of the 316LGBE specimen whose large grain size limited the mapping to approximately 265 grains. The OIM scans were performed with step sizes of less than one-tenth of the sample grain size, and hardness indentations made with a 25 g load were used as place markers. The indentation area and deformation region surrounding the indent with a radius of three times the diagonal length of the indent was excluded from all grain boundary character and cracking analyses. The boundaries were characterized according to Brandon's criterion [4], and the LABs were defined as having misorientations of 10°–15° and 5°–15° for the 316L and 690 specimens, respectively. All Σ3 boundaries, including coherent twins, are reported in the boundary fractions. The scans were run through two cleanup procedures to improve the quality of the grain boundary character maps. The first cleanup procedure identified points having a low confidence of being correctly indexed (confidence index of <0.2) and assigned those points the orientations of their neighboring points with the highest confidence indexes. The second procedure was used to restrict the minimum grain size to that of two times the scan step size. All grains below this size and points that could not be indexed were incorporated into the surrounding grain. In this paper, all reported grain boundary character distributions and cracked boundary fractions are reported as length fractions unless otherwise noted.

2.3. Constant extension rate tensile experiments

The four specimens underwent simultaneous constant extension rate tensile (CERT) experiments in 500 °C deaerated SCW at

Table 1
Chemical compositions of 316L and 690 (wt%).

Alloy	Fe	C	Mn	P	S	Si	Ni	Cr	Mo	Cu	Co	Nb	Al	Ti
316L	Bal	0.02	1.86	NM*	NM	0.5	10.1	16.6	2.1	0.24	0.1	NM	NM	NM
690	10.00	0.03	0.18	NM	0.001	0.03	Bal	29.4	0.01	0.01	NM	<0.01	0.22	0.34

* NM = not measured.

a pressure of 24 MPa. The dissolved oxygen content of the water was <10 ppb and the conductivity <0.10 μS/cm for the duration of the experiment. The samples were strained at a rate of $1 \times 10^{-7}\ s^{-1}$, and the experiment was interrupted at approximately 5%, 15%, and 25% nominal strain for analysis.

After each straining increment, the experiment was interrupted and the samples were analyzed at a magnification of 1000× with a JEOL JSM-6480 SEM. No intergranular cracks were found on the gage surfaces of the specimens at 5% strain, but quantitative measures of the average crack lengths, crack densities, and the crack length per unit areas on each specimen surface were recorded at 15% and 25% strain. All of the crack lengths on a specimen surface were included to yield the average crack length. In this study the crack length was defined as the total length of a continuous crack which often extended across several boundaries on the gage surface of the specimen. The crack densities were reported as the number of cracks per unit area of the gage surface. The crack length per unit area measurements accounted for both the crack length and crack density, and is the boundary length per unit area that has cracked on the gage surface. The character of each cracked grain boundary was determined by comparing the SEM micrographs to the grain boundary character maps. In this study, a grain boundary was defined as the boundary segment lying between two triple junctions, including coherent twin triple junctions.

The error bars in the *IGSCC behavior* section of this paper indicate the experimental uncertainty in the measurements. The uncertainty was determined by repeating crack measurements on the specimens and determining the percent variation in the crack length and density measurements. The uncertainty in the fractions of boundaries that cracked was estimated using an equation developed by Alexandreanu and Was [26] as indicated in Eq. (1) as

$$\frac{\sigma_{pc}}{p_c} = \left(\frac{1}{N_c} \frac{1-p_c}{p_c} + \left(\frac{\sigma_{pc}}{p_c} \right)^2_{\exp} \right)^{1/2}, \tag{1}$$

Table 2
Length fractions of boundary types in tensile specimens.

Alloy	LAB	Σ3	Σ9	Σ27	Special	RHAB
316L	0.031	0.438	0.010	0.003	0.482	0.518
316LGBE	0.010	0.599	0.038	0.013	0.660	0.340
690	0.022	0.575	0.025	0.003	0.625	0.375
690GBE	0.011	0.675	0.081	0.043	0.810	0.190

where p_c is the fraction of cracked boundaries and N_c is the total number of boundaries of a particular type. The uncertainty in the identification of grain boundary character and crack length was included in the experimental uncertainty, $\left(\frac{\sigma_{pc}}{p_c}\right)_{\exp}$. In this study, the length fraction of cracked boundaries was used for p_c, and N_c was calculated as follows:

$$N_c = \frac{y_c}{p_c}, \tag{2}$$

where y_c is the number of cracked boundaries of a particular type. This assumes that the length fraction and number fraction of boundaries cracked are equal.

3. Results

3.1. Grain boundary character distribution

The objective of the thermomechanical processing was to achieve two conditions for each alloy with largely different special boundary fractions in order to determine the influence of the special boundary fraction on the IGSCC susceptibility of the alloy. The special boundary length fractions in the specimens following thermomechanical processing are given in Table 2. The boundary types were grouped into two categories, RHABs and special boundaries (LABs, Σ3s, Σ9s, and Σ27s).

As shown in Table 2, the GBE specimens had higher special boundary fractions than the 316L and 690 specimens. The high Σ3 fraction in 690GBE (0.675) was roughly equal to the theoretical twin limit of 2/3 [27]. Also note that the length fractions of Σ9 and Σ27 boundaries increased with the fraction of Σ3 boundaries. This is consistent with literature which shows that as the fraction of Σ3 boundaries increases, the probability of Σ3 interaction during grain boundary migration increases and $\Sigma 3^n$ boundaries are created according to the joining and dissociation rules for CSLBs [28]. Representative grain boundary maps from the gage surfaces of the specimens are shown in Fig. 1. The large population of Σ3 coherent twin boundaries is characteristic of low stacking fault energy FCC metals and is evident in all four specimens. The two GBE specimens (the 690GBE specimen in particular), also had a substantial fraction of Σ3 boundaries that were not annealing twins. The differences in the grain sizes of the specimens can also be seen in Fig. 1. In addition to the higher special boundary fractions in the GBE specimens, the RHAB networks in the samples were disrupted as shown in the RHAB maps in Fig. 1. As discussed in the introduction, this type of fragmented RHAB network is desirable in preventing intergranular crack propagation.

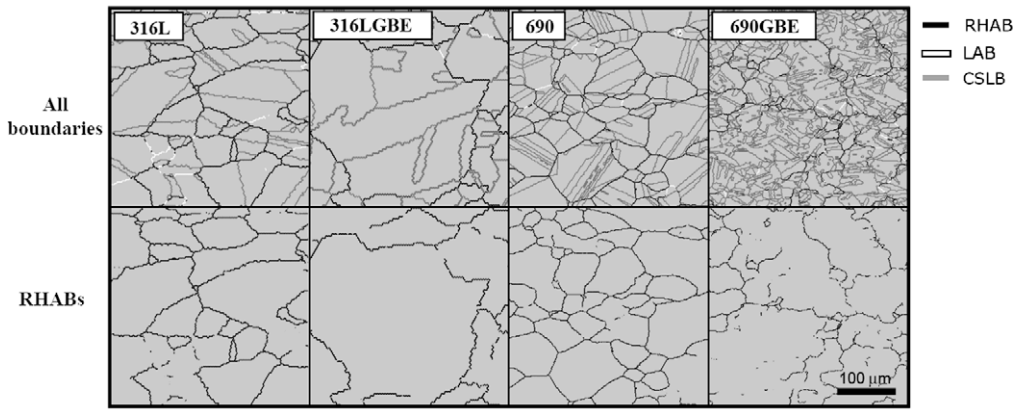

Fig. 1. Representative grain boundary character maps of gage surfaces of four tensile specimens.

Table 3
Plastic strain of each specimen following nominal straining to 5, 15, and 25%.

Nominal strain (%)	Plastic strain (%)			
	316L	316LGBE*	690	690GBE
5	4	7	4	4
15	13	16	13	13
25	23	27	23	22

* 316LGBE plastically yielded due to internal autoclave pressure.

3.2. IGSCC behavior

The 316LGBE specimen yielded plastically due to the internal autoclave pressure which exerted a stress of 121 MPa on the specimen resulting in a final plastic strain of 26.6% compared to the 22–23% strain experienced by the other specimens. The plastic strain of each specimen following each straining increment is given in Table 3. The cracks reported in this study were at least 1 μm in length, as this was the minimum resolvable crack length on the SEM at a magnification of 1000×. Analysis of the specimen gage surfaces revealed a substantial amount of SCC. The cracking on the 316L and 316LGBE specimens was mostly intergranular whereas the 690 specimens had a substantial amount of transgranular cracking in addition to intergranular cracking as shown in Fig. 2. Only the intergranular cracking is reported in the cracking analyses.

SEM analysis was performed on the gage surfaces of the tensile specimens to quantify their cracking behavior. Average crack length measurements on the specimens ranged from 10.5 to 48.5 μm as indicated in Fig. 3, and changed only slightly between 15% and 25% strain. It can be shown that the average crack length had a positive correlation with the specimen grain size as shown in Fig. 4.

Gage surface crack density measurements showed that the 690 and 690GBE specimens had higher intergranular crack densities than the 316L and 316LGBE specimens. Crack densities on the 316L, 316LGBE, 690, and 690GBE specimens increased by factors of 3, 11, 2, and 5, respectively, from 15 to 25% strain as shown in Fig. 5.

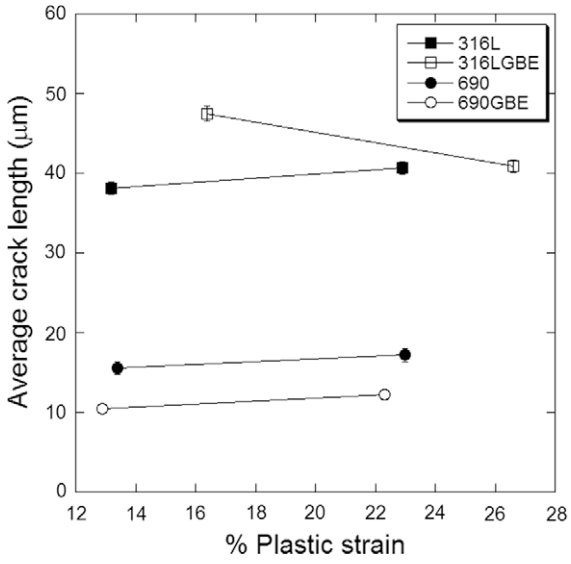

Fig. 3. Average crack lengths on gage surfaces of tensile specimens after straining to 15% and 25% in 500 °C SCW.

The crack length per unit area was a more cumulative measure of the cracking susceptibility and also increased dramatically with strain as shown in Fig. 6. The increase from 15% to 25% strain was largely due to the increase in crack density, as it was shown in Fig. 3 that there was only a minor change in average crack length from 15% to 25% strain. The crack length per unit area measurements from 15% to 25% strain increased by factors of 3, 10, 2 and 6 for the 316L, 316LGBE, 690, and 690GBE specimens, respectively. The total fraction of grain boundary length cracked in each speci-

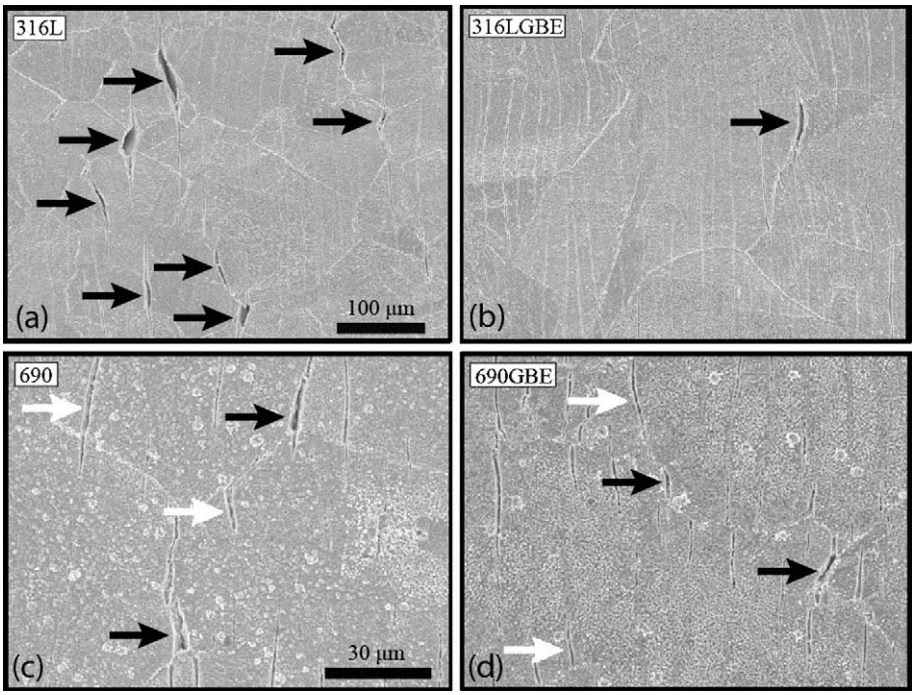

Fig. 2. SEM images of gage surfaces of specimens strained to 25% in 500 °C SCW. Black arrows indicate intergranular cracking and white arrows indicate transgranular cracking. The tensile direction is horizontal.

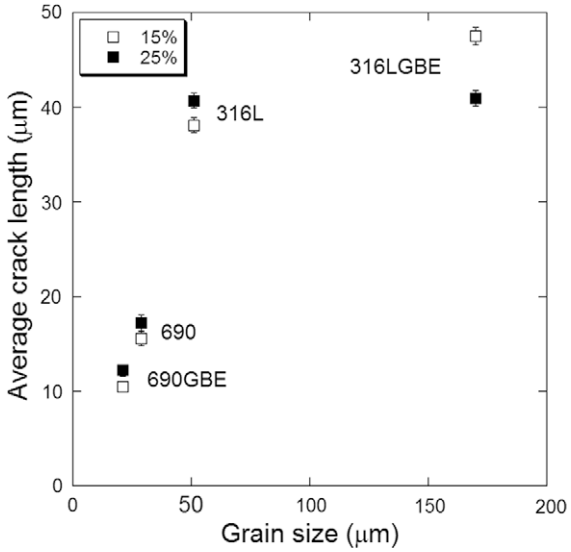

Fig. 4. Influence of specimen grain size on average crack length at 15% and 25% strain.

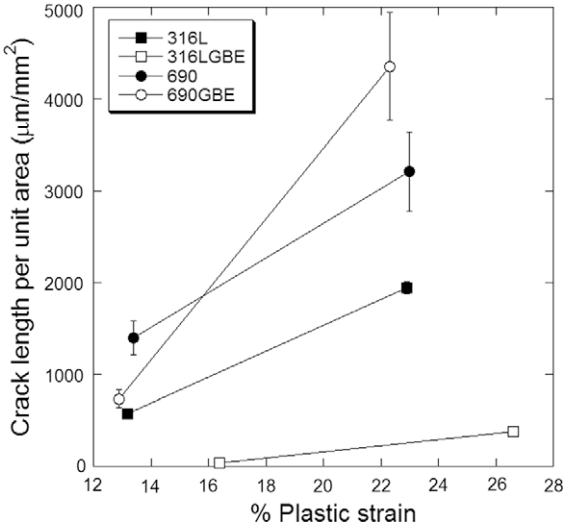

Fig. 6. Crack length per unit area on gage surfaces of tensile specimens after straining to 15% and 25% in 500 °C SCW.

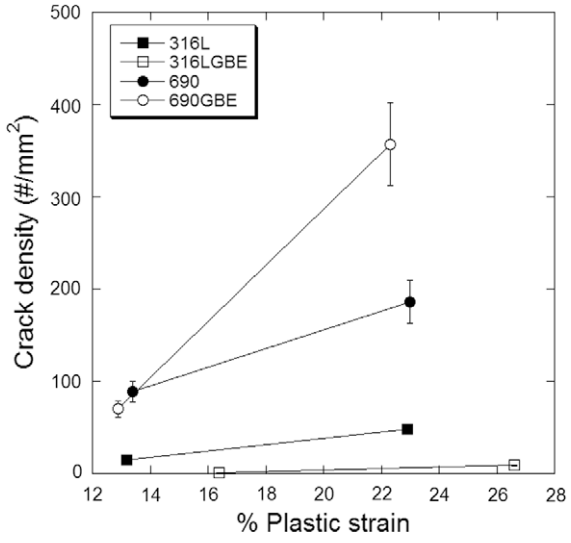

Fig. 5. Crack densities on gage surfaces of tensile specimens after straining to 15% and 25% in 500 °C SCW.

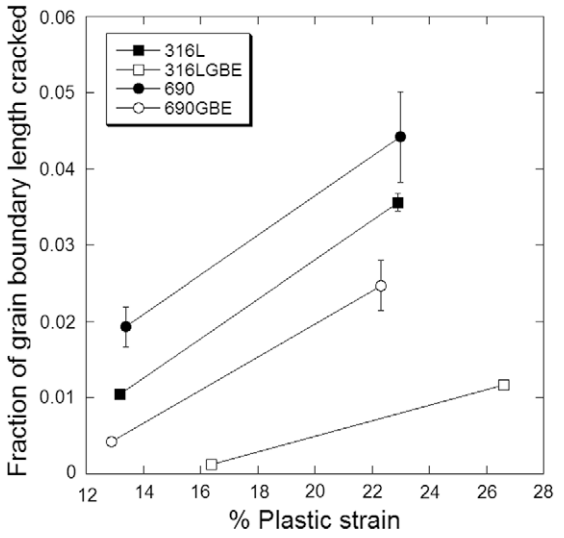

Fig. 7. Fraction of grain boundary length cracked on gage surfaces of tensile specimens after straining to 15% and 25% in 500 °C SCW.

men was determined by normalizing the crack length per unit area measurements to the total grain boundary length analyzed as shown in Fig. 7. Compared to the 316L and 690, the fraction of grain boundary length cracked in the 316LGBE and 690GBE specimens decreased by factors of 9 and 5 at 15% strain and 3 and 2 at 25% strain, respectively. Although the fraction of grain boundary length cracked never exceeded 5%, this was a substantial amount of cracking for these alloys.

3.3. IGSCC susceptibility of special boundaries

In addition to determining the overall cracking susceptibilities of the alloys, it was important to know the relative susceptibilities of the various boundary types. The length of each cracked boundary was measured and classified as either a RHAB or special boundary. The total length of cracked RHABs and special boundaries was compared to their total lengths in the areas analyzed to determine the fractions of each boundary type that cracked. These values indicated the frequency of IGSCC at a given point along either type of grain boundary and are shown in Fig. 8. At both 15% and 25% strain, the RHABs were more susceptible to IGSCC than the special boundaries. At 25% strain, the difference was a factor of 18, 10, 11, and 9 for the 316L, 316LGBE, 690, and 690GBE specimens, respectively.

Although special boundaries as a whole exhibit resistance to IGSCC, the specific types of special boundaries may not exhibit equal resistance. The limited number of cracked special boundaries made it difficult to confidently determine the relative cracking susceptibilities of each boundary character. There was sufficient data, however, to show that the LABs and $\Sigma 3$ boundaries were less susceptible than the RHABs, as illustrated in Fig. 9. The cracking frequency of a $\Sigma 3$ boundary or LAB was less than that of a RHAB in each alloy. Note that the large uncertainties in some of these measurements were due to the limited number of special boundaries that cracked, as indicated in Table 4.

As a consequence of the low, but non-zero susceptibility of special boundaries to IGSCC, it follows that the contribution of

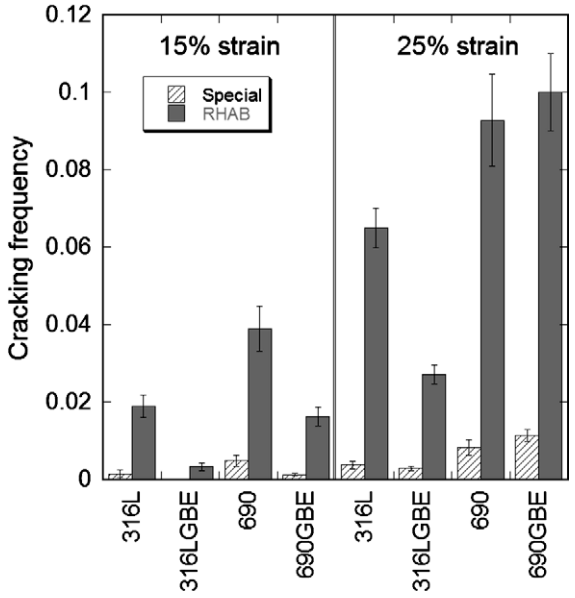

Fig. 8. Frequency of crack occurrence at special boundaries and RHABs following straining to 15% and 25% in 500 °C SCW.

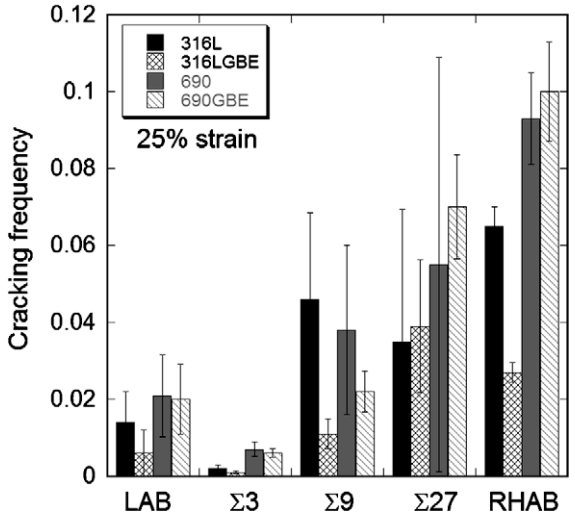

Fig. 9. Frequency of intergranular cracking at each type of special boundary and at RHABs after 25% strain in 500 °C SCW.

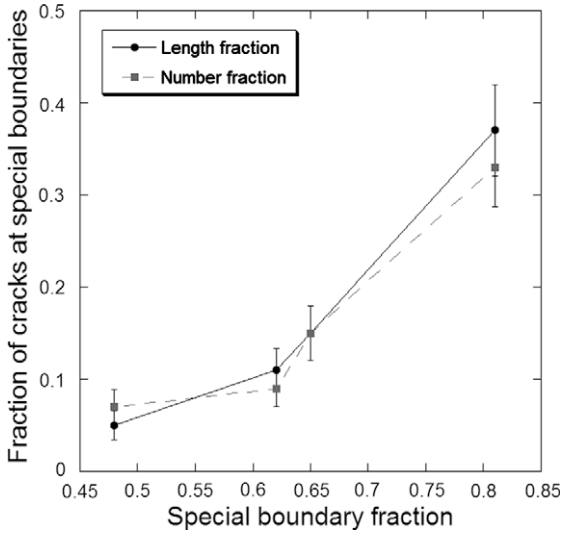

Fig. 10. Fraction of cracks at special boundaries versus total special boundary length fractions.

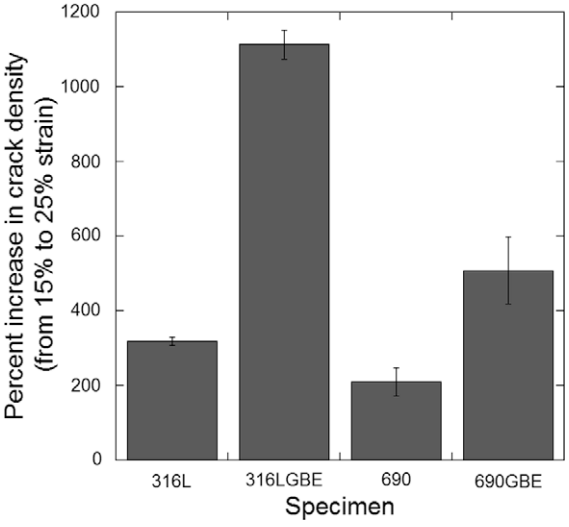

Fig. 11. Percent increase in crack density from 15% to 25% strain.

the special boundaries to the fraction of the *cracks* that occurred at special boundaries increases as the *total* special boundary fraction of the alloy increases. Consider that, although the susceptibility of special boundaries in 690GBE was a factor of 9 lower than that of the RHABs, 37% of the total crack length occurred along special boundaries. This seemingly contradictory observation is understood by considering that 81% of the total boundary length was contributed by special boundaries. Fig. 10 shows that both the length and number fraction of the cracks that occurred at special boundaries steadily increased with the special boundary fraction of the alloy. Note that the length and number fraction values were comparable.

Table 4
Number of cracked boundaries analyzed following straining to 15% and 25%.

Strain	Specimen	#Cracked RHABs	#Cracked LABs	#Cracked Σ3's	#Cracked Σ9's	#Cracked Σ27's
15%	316L	46	1	0	1	0
	316LGBE	11	0	0	0	0
	690	102	0	10	1	0
	690GBE	83	4	2	5	10
25%	316L	174	3	6	4	1
	316LGBE	123	1	8	8	5
	690	235	4	15	3	1
	690GBE	209	5	36	22	38

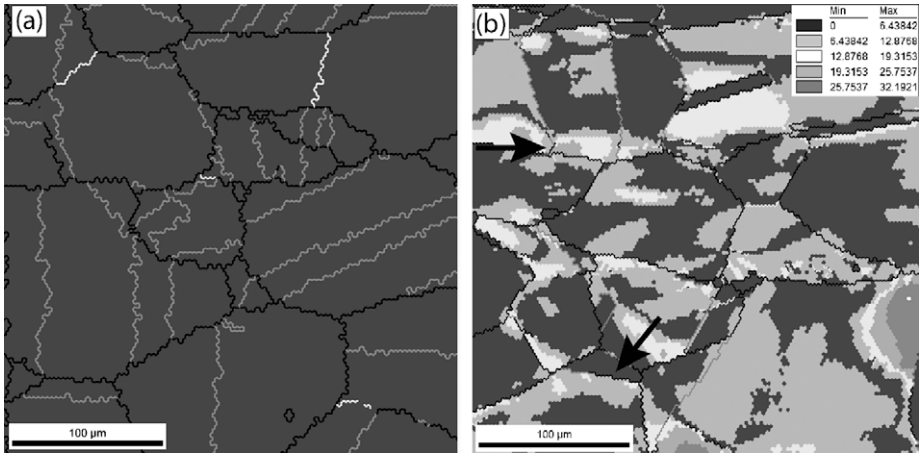

Fig. 12. Orientation deviation maps of 316L in (a) the undeformed condition, and (b) after 36% plastic strain in 400 °C argon. Arrows indicate boundaries that are not a single continuous character. Note that maps were generated from two different specimens. The tensile direction of the specimens is horizontal.

4. Discussion

These results show that in general, the average crack length, crack density, and crack length per unit area increased with strain level from 15% to 25%, Figs. 3–6. The average crack length of the 316LGBE was the only exception to this trend in that it decreased with strain as was shown in Figs. 3 and 4. The average crack length for the specimen as a whole can decrease if new cracks are formed. Fig. 11 shows that the crack density of the 316LGBE specimen increased more dramatically from 15% to 25% strain than the rest of the specimens. The tendency of 316LGBE to nucleate new cracks rather than propagate existing cracks may be responsible for the decrease in average crack length.

Crack length increased with grain size. The increase, shown in Fig. 4, was likely due to the lower density of triple junctions present in alloys with larger grain sizes. Kumar et al. [29] and Marrow et al. [30] have shown that triple junctions can act as sites of crack arrest, especially if they consist of one or more special boundaries. Marrow observed crack bridging ligaments that failed in a ductile manner at high strains and postulated that they were created by the intersection of a low Σ CSLB that associated with a twin during recrystallization. In this study, it was determined that, at 25% strain, over 50% of the cracks in each of the four specimens did not propagate through a single triple junction. It is therefore likely that the higher density of triple junctions in the smaller grain specimens acted as sites of crack arrest and limited the average crack length.

Both the crack density and crack length per unit area increase with strain. The effects of GBE on these values, however, were not easily seen in Figs. 5 and 6, because the influence of grain size had not been accounted for. Alloys with smaller grain sizes have more grain boundary length per unit area of the sample surface. Therefore, there are more potential sites for intergranular cracking in specimens with small grains. The fraction of cracked grain boundary length, shown in Fig. 7, accounts for the density of grain boundaries and more clearly illustrates the effects of GBE. Recall that the 316LGBE had a larger grain size than the 316L, and the 690GBE had a smaller grain size than the 690. These results show that, regardless of whether GBE increases or decreases grain size, the total fraction of grain boundary length cracked will decrease as the special boundary fraction increases.

These results confirmed that GBE was effective in reducing IGSCC in supercritical water. The IGSCC resistance of the special boundaries showed that they are responsible for the improvement in cracking behavior. Recall that, at 25% strain the special boundaries were 9–18 times less likely to crack than RHABs. In this study, LABs, Σ3, Σ9, and Σ27 boundaries were categorized as special, however, only LABs and Σ3 boundaries were confirmed to be superior to RHABs as was illustrated in Fig. 9. It is well-established that CSLBs are not immune to cracking. Studies have reported special boundaries cracking in a variety of environments: 10% NaOH at 350 °C [16], simulated primary water [8], 360 °C deaerated water [15], and even argon [17]. There is no universally accepted limit for the Σ boundaries that can be considered special, and there are factors other than misorientation that can affect the susceptibility of the boundary to IGSCC, including the crystallographic orientation of the grain and the grain boundary plane. Therefore, even boundaries of the same character may exhibit varying resistance to IGSCC.

The results from this study and of others [8,17] suggest that as damage accumulates under strain, even more resistant boundaries can ultimately fail. Therefore, the effects of GBE are more evident at lower strains. Comparisons of the cracking in the 316L and 316LGBE specimens, and the 690 and 690GBE specimens, showed that GBE decreased cracking by factors of 9 and 5 at 15% strain, and by factors of 3 and 2 at 25% strain, respectively. This decrease in IGSCC resistance of the GBE specimens at 25% strain is consistent with the cracking behavior of Ni–16Cr–9Fe–*x*C reported by Alexandreanu et al. [8]. The effect of the CSL enhancement on the cracking behavior in Alexandreanu's study was greater at 15% and 20% strain, and by 25% it was reported that the grain boundary character was not as important. One possible cause of the decrease in effectiveness with strain is a change in grain boundary misorientation due to grain rotation. Fig. 12 compares grain boundary maps of a 316L specimen in the annealed condition and a specimen that had been strained to 36% in 400 °C argon. The maps illustrate how the orientations of specific points within a grain deviate from the average orientation of the grain. Note that all of the Σ3 boundaries in the annealed condition (12a) are continuous, whereas in the deformed condition (12b), several are interrupted by segments of RHABs as indicated with arrows. All of the grain boundary maps in the present study were generated prior to straining, so it is possible that grain rotation may have changed the grain boundary misorientation to convert special boundaries to RHABs prior to fracture.

5. Conclusions

GBE of 316L stainless steel and alloy 690 reduced the fraction of grain boundary length cracked in 500 °C supercritical water. This

reduction was due to the presence of a high fraction of IGSCC resistant special boundaries. LABs and Σ3 boundaries were less susceptible to IGSCC than RHABs, but the superiority of Σ9 and Σ27 boundaries could not be confirmed. The average crack length on the gage surfaces of the specimens correlated with grain size and was likely due to the higher densities of triple junctions in small grain size samples, which acted as barriers to crack advance. GBE was more effective at reducing cracking propensity at lower strains.

Acknowledgements

The authors wish to thank the staff of the University of Michigan Electron Microbeam Analysis Laboratory (EMAL) for use of the EBSD equipment. This research was supported by NERI award #DE-FC07-05ID14664 for Project Number 05-151.

References

[1] G.S. Was, P. Ampornrat, G. Gupta, S. Teysseyre, E.A. West, T.R. Allen, K. Sridharan, L. Tan, Y. Chen, X. Ren, C. Pister, J. Nucl. Mater. 371 (2007) 176.
[2] S. Teysseyre, Z. Jiao, E. West, G.S. Was, J. Nucl. Mater. 371 (2007) 107.
[3] H. Grimmer, W. Bollmann, D.H. Warrington, Acta Crystallogr. A30 (1974) 197.
[4] D.G. Brandon, Acta Metall. 14 (1966) 1479.
[5] L. Hongwei, G. Ming, D.G. Harlow, R.P. Wei, Scr. Metall. 32 (1995) 1807.
[6] S. Watanabe, Y. Takamatsu, N. Sakaguchi, H. Takahashi, J. Nucl. Mater. 283–287 (2000) 152.
[7] J.J. Kai, F.R. Chen, T.S. Duh, Mater. Trans. 45 (2004) 40.
[8] B. Alexandreanu, B. Capell, G.S. Was, J. Mater. Sci. Eng. 300 (2001) 94.
[9] T. Watanabe, S. Kitamura, S. Karashima, Acta Metall. 28 (1980) 455.
[10] P. Lin, G. Palumbo, U. Erb, K.T. Aust, Acta Metall. 33 (1995) 1387.
[11] M. Shimada, H. Kokawa, Z.J. Wang, Y.S. Sato, I. Karibe, Acta Mater. 50 (2002) 2331.
[12] G. Palumbo, K.T. Aust, Acta Metall. 38 (1990) 2343.
[13] M. Michiuchi, H. Kokawa, Z.J. Wang, Y.S. Sato, K. Sakai, Acta Mater. 54 (2006) 5179.
[14] G.S. Was, V. Thaveeprungsriporn, D.C. Crawford, JOM 50 (1998) 44.
[15] Y. Pan, B.L. Adams, T. Olson, N. Panayotou, Acta Mater. 44 (1996) 4685.
[16] G. Palumbo, K.T. Aust, E.M. Lehockey, U. Erb, P. Lin, Scr. Mater. 38 (1998) 1685.
[17] D.C. Crawford, G.S. Was, Metall. Trans. 23A (1992) 1195.
[18] E.M. Lehockey, G. Palumbo, Mater. Sci. Eng. A237 (1997) 168.
[19] T. Watanabe, Res. Mech. 11 (1984) 47.
[20] T. Watanabe, J. Mater. Sci. Eng. A176 (1994) 39.
[21] V.Y. Gertsman, K. Tangri, Acta Mater. 45 (1997) 4107.
[22] V. Randle, Acta Mater. 52 (2004) 4067.
[23] L. Tan, K. Sridharan, T.R. Allen, R.K. Nanstad, D.A. McClintock, J. Nucl. Mater. 374 (2008) 270.
[24] L. Tan, K. Sridharan, T.R. Allen, J. Nucl. Mater. 348 (2006) 263.
[25] G. Gupta, P. Ampornrat, X. Ren, K. Sridharan, T.R. Allen, G.S. Was, J. Nucl. Mater. 361 (2007) 160.
[26] B. Alexandreanu, G.S. Was, Philos. Mag. A 81 (2001) 1951.
[27] G. Palumbo, K.T. Aust, U. Erb, P.J. King, A.M. Brennenstuhl, P.C. Lichtenberger, Phys. Status Solidi A 131 (1992) 425.
[28] V. Randle, Acta Mater. 47 (1999) 4187.
[29] M. Kumar, W.E. King, A.J. Schwartz, Acta Mater. 48 (2000) 2081.
[30] T.J. Marrow, L. Babout, A.P. Jivkov, P. Wood, D. Engelberg, N. Stevens, P.J. Withers, R.C. Newman, J. Nucl. Mater. 352 (2006) 62.